Location Sensitivity in Multipath Environment

M. João D. Rendas*

José M. F. Moura

LASIP, Depart. Elect. and Comp. Eng., Carnegie Mellon University, Pittsburgh, PA, 15213.

Abstract

The work is concerned with the location of submerged objects when a bilinear approximation to the propagation velocity profile in the ocean is used. Contrasting with isovelocity profiles, there are available multiple refracted as well as reflected rays which when resolved provide the required information to determine the range and depth source parameters. The paper establishes the Cramer–Rao bounds for the errors associated with depth and range in positioning systems for a particular configuration, considering observations in a single sensor, for a multipath channel with a bilinear velocity profile.

1. Introduction

In [9], we derived performance bounds for the localization problem for the simple channel with a single direct path between the source and the receiver. In practice, however, the propagation structure is much more complex. Under certain geometric conditions, also related to the frequency contents of the signals, the propagated field is approximated by ray theory, which predicts the existence of multiple rays between the object and the receiver. Herein, we use this approximation to model the ocean's effect on the radiated signal. Alternative methods, using mode propagation [5], [2], or matched field processing [1], [4] have also been considered for performance analysis in location problems. By restricting attention to ray theory, we focus on relevant issues of multipath while still being able to pursue analytical and quantitative results that seem to defy other competing approaches.

Bounds for the error in delay estimation when two or three paths are present are studied in [6] and [3]. The latter work also discusses bounds for range and depth for an isovelocity propagation channel with two pathes – a direct path and either a surface or bottom bounce. This is rather unrealistic in underwater when the source/receiver pair are separated by more than a few nautical miles.

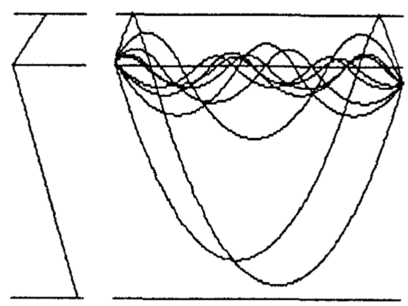

Figure 1: Ray structure, velocity profile.

We derive bounds for the errors in range and depth estimation using a bilinear approximation to the velocity profile. We use the propagation parameterization and algorithm in [7]. Figure 1 sketches the velocity profile and the basic ray structure: refracted rays, surface and/or bottom reflected rays. The type and number of rays present depend on the specific geometry considered.

Besides the actual structure of the estimation algorithm, relevant questions regard the performance and sensitivity of the technique, namely (i) what is the associated ambiguity structure, i.e., the probability of large or decision errors; (ii) what is the "best" one can do in a mean square sense when no decision errors are made; (iii) what is the sensitivity of the technique to prior modeling assumptions.

A preliminary study of the implications of item (i) is in [8]. We will tackle here item (ii) by deriving Cramer-Rao bounds. The dependence of the bounds on geometry and environmental parameters is derived for particular configurations. This is insightful not being readily available with other approaches. It will be clear from the results that the parameterization developed here allows the consideration in a quantitative as well as qualitative way of sensitivity issues. This will be more fully explored elsewhere.

*visiting, on leave from CAPS, Instituto Superior Técnico, Lisbon, Portugal, on a fellowship from INVOTAN, Portugal.

Section 2 describes the propagation model and the algorithm presented in [7]. Section 3 applies this algorithm to a particular configuration for which we can find analytical parameterizations for the delays and derivatives of the delays with respect to range and depth. These expressions are used in section 4 to derive the Cramer-Rao bound for the range/depth variables. Section 5 summarizes the results.

2. Bilinear Velocity Profile

We assume that the ocean is a linear medium, that there is horizontal homogeneity, namely the velocity profile is a function of depth only, that there are no random fluctuations in the channel propagation, and that the medium boundaries are plane.

Using ray acoustics, and not taking into account the dispersive character of the medium, the ocean is equivalent to a parallel of delay/attenuation all pass linear filters each one corresponding to a ray between the emitting and receiving points. To preserve the analytical tractability of the problem, we consider here a bilinear profile (see Figure 1). For mediums with this type of refractive index variation, the energy is trapped about the depth of the minimum propagation velocity due to the continuous refraction of the "acoustic rays." Contrasting with the predictions of the simple constant speed models, multiple rays are allowed to exist between given points. We group them into purely refracted rays (SOFAR), surface reflected rays (SR), surface/bottom reflected rays (SBR), and bottom reflected rays (BR).

In this study, we ignore the availability of bottom bounced rays (SBR and BR). This is appropriate whenever the power loss at the ocean/bottom interface is large. The algorithm of [7] can be used in the general case that includes SBR and BR rays.

The rays are parameterized according to the number K of complete bounces about the duct's axis. We present below several analytical expressions relating geometric parameters describing the source/receiver configuration and the installed rays. For simplicity, the expressions assume that both source and receiver are above the duct's axis. Expressions for the general case can be found in [7].
SOFAR rays:

$$R = \frac{v_s}{g_0}\tan(\theta_s) + A_1 v_0|\tan(\theta_0)| - \frac{v_r}{g_0}\tan(\theta_r) \quad (1)$$

SR rays:

$$\begin{aligned} R = \; & \tfrac{v_s}{g_0}\tan(\theta_s) + A_1 v_0|\tan(\theta_0)| \\ & -A_2\tfrac{v_{sur}}{|g_0|}|\tan(\theta_{sur})| - \tfrac{v_r}{g_0}\tan(\theta_r) \end{aligned} \quad (2)$$

where v_s, v_r, v_0, v_{sur} are, respectively, the velocities at the source, receiver, duct (minimum velocity), and surface levels; θ_s, θ_r, θ_0, θ_{sur} are the ray angles at the source (launching), at the receiver, at the duct, and at the surface, respectively; g_0, g_1 are the velocity gradients above and below the duct — note $g_0 < 0$, while $g_1 > 0$; g is an equivalent gradient given by the parallel combination of the two, i.e.,

$$\frac{1}{g} = \frac{1}{|g_0|} + \frac{1}{g_1}; \quad (3)$$

K is the number of complete bounces; δ is the sign of the receiving angle; A_1 and A_2 are

$$A_1 = 2(K+1)\tfrac{1}{g}$$

$$A_2 = \begin{cases} 2K & \theta_s > 0, \theta_r < 0 \\ 2(K+1) & \theta_s\theta_r > 0 \\ 2(K+2) & \theta_s < 0, \theta_r > 0. \end{cases} \quad (4)$$

All angles are measured clockwise with respect to the horizontal. For rays not crossing the duct, both equations have to be modified. Details are omitted.

Using Snell's law to relate the several angles in equation (1) yields a 4th degree equation in $\tan(\theta_s)$ from which the SOFAR rays with a given value for K are determined. Proceeding similarly with equation (2), an 8th degree polynomial equation in $\tan(\theta_s)$ is obtained. We point out that the dependence of A_2 on the signs of the emitter and receiving angles leads to separate equations for a single value of K, in contrast to what happens with the SOFAR rays for which the mentioned 4th degree polynomial's roots give all the possible SOFAR rays for a given K.

The number of eigenrays between any two given points is a complex function of their particular location, but it varies between 0 and 4 for SOFAR rays, and 0 and 8 for surface reflected rays.

Finally, the propagation parameters are easily parameterized in terms of the launching angle. Here, we will not consider the variation of the attenuation parameter, so that of concern is only the path delay. The complete treatment will be provided elsewhere.

For SOFAR rays,

$$\tau(\theta_s) = \tau_s + 2(K+1)(\tau_0 + \tau_1) + \tau_r \quad (5)$$

where

$$\tau_s = \tfrac{\gamma}{g_0}\mathcal{F}(c_s), \quad \tau_i = \tfrac{1}{|g_i|}\mathcal{F}(c_0), \quad \tau_r = -\tfrac{\delta}{g_0}\mathcal{F}(c_r) \quad (6)$$

where we used the short-hand notations

$$c_x = \cos(\theta_x), \quad \mathcal{F}(x) = \ln\left|\tfrac{1+\sqrt{1-x^2}}{x}\right| \quad (7)$$

For SR rays the delays are determined in a similar manner. The general expression (for rays that cross the duct) is:

$$\tau(\theta_s) = \tau_s + 2(K+1)(\tau_0 + \tau_1) - A_2\tau_{sur} + \tau_r \qquad (8)$$

where

$$\tau_{sur} = \frac{1}{|g_0|}\mathcal{F}(c_{sur}). \qquad (9)$$

3. Equal Source/Receiver Depth

There are configurations for which the results are particularly simple. We discuss in this section one of these, namely when source and receiver are located at the same depth. Other configurations for which analytical results can be obtained include those where either source or receiver are at the surface, and those where either one is at the duct axis. Lack of space prevents us from pursuing these here.

For equal depth, $v_s = v_r$, which implies $|\theta_s| = |\theta_r|$. Substituting in equation (1), we get for the SOFAR direct ray:

$$R = \frac{2v_s}{g_0}\tan(\theta_s) \qquad (10)$$

and for the other SOFAR rays,

$$R = \frac{v_s}{g_0}(1+\epsilon)\tan(\theta_s) + v_0 A_1 |\tan(\theta_0)|. \qquad (11)$$

Working with (2), leads for the surface reflected rays

$$R = \frac{v_s}{g_0}(1+\epsilon)\tan(\theta_s) + v_0 A_1 |\tan(\theta_0)| + \frac{v_{sur}}{g_0} A_2 |\tan(\theta_{sur})| \qquad (12)$$

while for the "direct" surface ray

$$R = \frac{2v_s}{g_0}\tan(\theta_s) + 2\frac{v_{sur}}{g_0}|\tan(\theta_{sur})|. \qquad (13)$$

In the above equations, the parameter ϵ stands for

$$\epsilon = \begin{cases} 1 & \theta_s.\theta_r < 0 \\ -1 & \theta_s.\theta_r > 0. \end{cases} \qquad (14)$$

After algebraic manipulations, we obtain the parameterizations for the angles and delays in Tables I and II. Table III shows the derivatives of the SOFAR launching angles. Lack of space precludes the presentation here of the equations for the derivatives of the launching angles of the SR rays. The derivatives of the delays with respect to range R and depth Y are in Tables IV. In Tables I - IV symbol $*$ signals the direct rays (those that do not cross the duct), ans γ stans for the signal of the launching angle.

Table I.A — Sofar Launching Angles

ϵ	Angle ($z \triangleq \tan(\theta_s)$)
*	$\theta_s = \tan^{-1}(\frac{Rg_0}{2v_s})$
−1	$\theta_s = \cos^{-1}\left(\frac{A_1 v_s}{(R^2+v_0^2A_1^2)^{1/2}}\right)$
1	$a_0 + a_1 z + a_2 s z^2 = 0$ $a_0 = R^2 - A_1^2(v_s^2 - v_0^2)$ $a_1 = -4R\frac{v_s}{g_0}$ $a_2 = v_s^2(\frac{4}{g_0^2} - A_1^2)$

Table I.B — SR Launching Angles

ϵ	Angle ($z \triangleq \tan(\theta_s)$)
*	$\theta_s = \tan^{-1}\left(\frac{R^2+\frac{4}{g_0^2}(v_{sur}^2-V_s^2)}{4R\frac{v_s}{g_0}}\right)$
−1	$a_0 + a_1 z + a_2 z^2 = 0$ $a_0 = R^2 + \frac{A_2^2}{g_0^2}(v_{sur}^2 - v_0^2)$ $a_1 = -2Rv_0A_1$ $a_2 = v_0^2(A_1^2 - \frac{A_2^2}{g_0^2})$
1	$a_0 + a_1 z + a_2 z^2 + a_3 z^3 + a_4 z^4 = 0$ $a_0 = X^2 - 4A_1^2R^2(v_s^2 - v_0^2)$ $a_1 = 8R\frac{v_s}{g_0}[2A_1^2(v_s^2 - v_0^2) - X]$ $a_2 = 16\frac{v_s^2}{g_0^2}[R^2 - A_1^2(v_s^2 - v_0^2)]$ $+2XY - 4A_1^2R^2v_s^2$ $a_3 = 8R\frac{v_s}{g_0}(2A_1^2v_s^2 - Y)$ $a_4 = Y^2 - 16A_1^2\frac{v_s^2}{g_0^2}v_s^2$ $X = R^2 + A_1^2(v_s^2 - v_0^2) - \frac{A_2^2}{g_0^2}(v_s^2 - v_{sur}^2)$ $Y = v_s^2[A_1^2 + \frac{1}{g_0^2}(4 - A_2^2)]$

Table II.A — SOFAR Delays.

ϵ	τ
*	$\frac{2\gamma}{g_0}\mathcal{F}(c_s)$
−1	$A_1 \ln \left\| \frac{(R^2+v_0^2A_1^2)^{1/2}+R}{v_0A_1} \right\|$
1	$\frac{2\gamma}{g_0}\mathcal{F}(c_s) + A_1\mathcal{F}(c_0)$

Table II.B — SR Delays.

ϵ	τ
*	$\frac{2\gamma}{g_0}\mathcal{F}(c_s) + \frac{A_2}{g_0}\mathcal{F}(c_{sur})$
−1	$A_1\mathcal{F}(c_0) + \frac{A_2}{g_0}\mathcal{F}(c_{sur})$
1	$\frac{2\gamma}{g_0}\mathcal{F}(c_s) + A_1\mathcal{F}(c_0) + \frac{A_2}{g_0}\mathcal{F}(c_{sur})$

Table III — SOFAR Angle Derivatives.

ϵ	SOFAR
*	$\frac{\partial\theta_s}{\partial R} = \frac{g_0}{2v_s} \quad \frac{\partial\theta_s}{\partial Y} = \frac{Rg_0^2}{2v_s^2}$
−1	$\frac{\partial\theta_s}{\partial R} = \gamma\frac{A_1v_sR}{(R^2+v_0^2A_1)(R^2-A_1^2(v_s^2-v_0^2))^{1/2}}$ $\frac{\partial\theta_s}{\partial Y} = -\gamma\frac{Ag_0}{(R^2-A_1^2(v_s^2-v_0^2))^{1/2}}$
1	$\frac{\partial\theta_s}{\partial R} = -\frac{4\frac{v_s}{g_0}z+2R}{2a_2z+a_1}$ $\frac{\partial\theta_s}{\partial Y} = -\frac{g_0}{v_s}z + \frac{2A_1^2v_sg_0}{2a_2z+a_1}$

Table IV.A — SOFAR Delay derivatives.

ϵ	SOFAR
$*$	$\frac{\partial \tau}{\partial R} = -\tan(\theta_s)\frac{\partial \theta_s}{\partial R}\frac{2}{g_0\lvert\sin(\theta_s)\rvert}$ $\frac{\partial \tau}{\partial Y} = -\tan(\theta_s)\frac{\partial \theta_s}{\partial Y}\frac{2}{g_0\lvert\sin(\theta_s)\rvert}$
-1	$\frac{\partial \tau}{\partial R} = \frac{A_1}{(R^2+v_0^2A_1^2)^{1/2}} \qquad \frac{\partial \tau}{\partial Y} = 0$
1	$\frac{\partial \tau}{\partial R} = \tan(\theta_s)\frac{\partial \theta_s}{\partial R}\left[-\frac{2}{g_0\lvert\sin(\theta_s)\rvert} + \frac{A_1}{\lvert\sin(\theta_0)\rvert}\right]$ $\frac{\partial \tau}{\partial Y} = \tan(\theta_s)\frac{\partial \theta_s}{\partial Y}\left[-\frac{2}{g_0\lvert\sin(\theta_s)\rvert} + \frac{A_1}{\lvert\sin(\theta_0)\rvert}\right] + \frac{A_1 g_0}{v_s\lvert\sin(\theta_s)\rvert}$

Table IV.B — SR Delay derivatives.

ϵ	SR
$*$	$\frac{\partial \tau}{\partial R} = \tan(\theta_s)\frac{\partial \theta_s}{\partial R}\left[-\frac{2}{g_0\lvert\sin(\theta_s)\rvert} + \frac{A_2}{g_0\lvert\sin(\theta_{sur})\rvert}\right]$ $\frac{\partial \tau}{\partial Y} = \tan(\theta_s)\frac{\partial \theta_s}{\partial Y}\left[\frac{2}{g_0\lvert\sin(\theta_s)\rvert} + \frac{A_2}{g_0\lvert\sin(\theta_{sur})\rvert}\right] + \frac{A_2}{v_s\lvert\sin(\theta_s)\rvert}$
-1	$\frac{\partial \tau}{\partial R} = \tan(\theta_s)\frac{\partial \theta_s}{\partial R}\left[A_1\frac{1}{\lvert\sin(\theta_0)\rvert} + \frac{A_2}{g_0\lvert\sin(\theta_{sur})\rvert}\right]$ $\frac{\partial \tau}{\partial Y} = 0$
1	$\frac{\partial \tau}{\partial R} = \tan(\theta_s)\frac{\partial \theta_s}{\partial R}\left[-\frac{2}{g_0\lvert\sin(\theta_s)\rvert} + \frac{A_1}{\lvert\sin(\theta_0)\rvert} + \frac{A_2}{g_0\lvert\sin(\theta_{sur})\rvert}\right]$ $\frac{\partial \tau}{\partial Y} = \tan(\theta_s)\frac{\partial \theta_s}{\partial Y}\left[-\frac{2}{g_0\lvert\sin(\theta_s)\rvert} + \frac{A_1}{\lvert\sin(\theta_0)\rvert} + \frac{A_2}{g_0\lvert\sin(\theta_{sur})\rvert}\right] + \frac{A_1 g_0}{v_s\lvert\sin(\theta_0)\rvert} + \frac{A_2}{v_s\lvert\sin(\theta_{sur})\rvert}$

To use these results, we determine the values of K that occur for a given source/receiver configuration. For a given value of K and for fixed depth Y of the source and receiver, there is an interval of R where either SOFAR or SR rays with the given value of K exist. Figure 2 shows a plot of R as a function of θ_s. This plot, parameterized by ϵ, indicates the ranges and types of rays that can exist with a given launching angle θ_s. As mentioned earlier, at a given range there exists in between 0 and 4 rays. For a given K, the interval of R, $R_{int}(K)$, for which at least one ray exists, is determined from the above equations. Figure 3 shows a plot of the number of SOFAR rays, the horizontal axis is horizontal distance while the vertical axis is the depth common to both receiver and emitter. One should note that although there may be up to 4 SOFAR rays and up to 8 surface rays, these do not always correspond to distinct time delays and consequently to the parameter P in the propagation model of section 2. Namely, the time delay for the two rays with $\epsilon = -1$ is independent of the sign of the launching angle so that they are seen as the same arrival. These rays are not counted twice in plot 3.

4. Cramer Rao Bound

The Cramer-Rao bound (CRB) is presented for the configuration of section 3. Note that the bound is

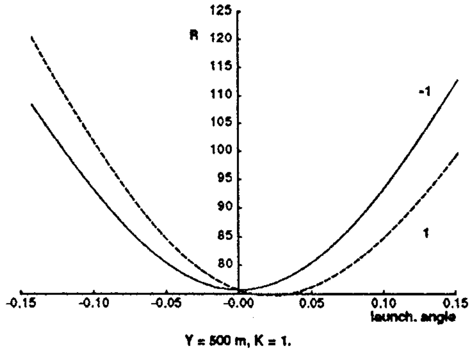

Figure 2: Interval of R (SOFAR rays).

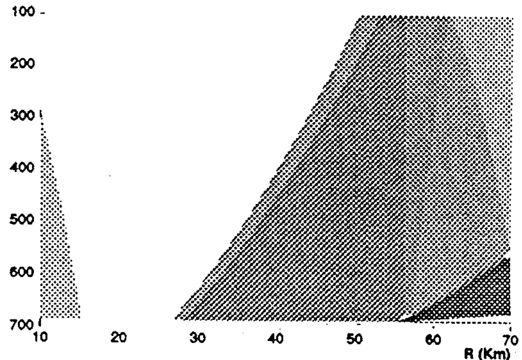

Figure 3: Number of SOFAR rays.

developed for a single sensor, so that range and depth information is recovered from the interpath delays, not from the wavefront curvature. The bounds for the latter case and using a single direct path propagation model were developed in [9]. The signal received at the sensor of known localization is

$$\begin{aligned} r(t) &= z(t) + n(t), \qquad t \in T \\ z(t) &= \textstyle\sum_{p=1}^{P} a_p s(t-\tau_p) \end{aligned} \tag{15}$$

where the propagation parameters a_p, τ_p, and P all depend on the source location vector $\Theta = [R, Y]$. Differences in attenuation are neglected except for a surface reflection coefficient whose magnitude may be taken smaller than 1. The CRB is [10]

$$\mathrm{CRB}(\Theta) = J(\Theta)^{-1} \tag{16}$$

where $J(\Theta)$ is the Fisher Information matrix (FIM). For sampled observations, $J(\Theta)$ is given asymptotically by [11], [3]

$$[J(\Theta)]_{ij} = \frac{N}{4\pi}\int_0^{2\pi} \mathrm{tr}\left[\frac{\partial \mathcal{S}_r(\omega)}{\partial \theta_i}\mathcal{S}_r^{-1}(\omega)\frac{\partial \mathcal{S}_r(\omega)}{\partial \theta_j}\mathcal{S}_r^{-1}(\omega)\right] d\omega. \tag{17}$$

Note that $\mathcal{S}_r(\omega)$ is the power spectral density (psd) of the received signal which is a discrete time signal; N is the number of samples, related to the time bandwidth product by $N = 2BT$, B being the single-side bandwidth in Hz. It is easy to see that

$$\mathrm{CRB}(\Theta) = \frac{\partial D}{\partial \Theta}^T \mathrm{CRB}(D)^{-1}\frac{\partial D}{\partial \Theta} \tag{18}$$

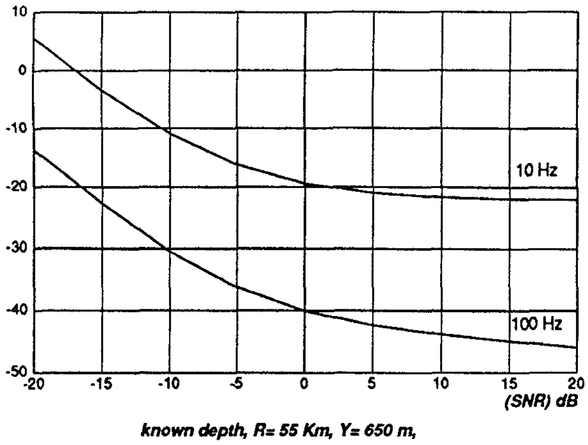

Figure 4: var(R)– Table V. Known depth.

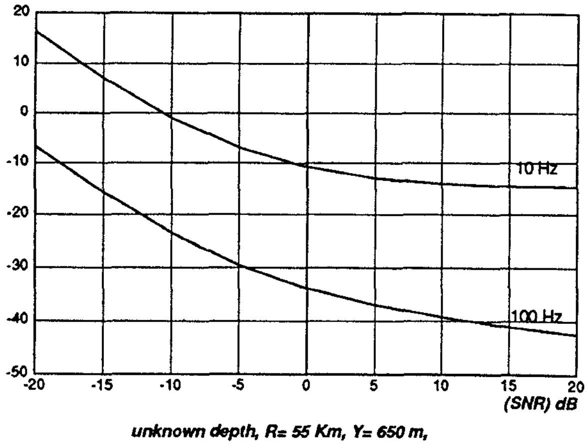

Figure 5: var(R)– Table V. Unknown depth.

where CRB(D) is the CRB for the estimation of the delays $\{\tau_p\}_{p=1}^{P}$, and $\frac{\partial D}{\partial \Theta}$ is the Jacobian matrix:

$$\frac{\partial D}{\partial \Theta} \triangleq \begin{bmatrix} \frac{\partial \tau_1}{\partial R} & \frac{\partial \tau_1}{\partial Y} \\ \vdots & \vdots \\ \frac{\partial \tau_P}{\partial R} & \frac{\partial \tau_P}{\partial Y} \end{bmatrix} \quad (19)$$

For additive noise, uncorrelated with the transmitted signal, $\mathcal{S}_r(\omega) = \mathcal{S}_z(\omega) + \mathcal{S}_n(\omega)$, where $\mathcal{S}_n(\omega)$ is the psd of the noise and

$$\mathcal{S}_z(\omega) = \mathcal{S}_s(\omega)\mathbf{a}^T E(\omega)\mathbf{a}, \quad (20)$$

where $\mathbf{a} = [a_1, \ldots, a_P]$, and

$$[E(\omega)]_{ij} = e^{j\omega(\tau_i - \tau_j)}, \qquad i,j = 1,\ldots,P. \quad (21)$$

In (20), $\mathcal{S}_s(\omega)$ is the psd of $s(t)$. Differentiating with respect to τ_i yields the following expression for the FIM of the delays:

$$J(D) = \mathrm{diag}\{a_i\} K \mathrm{diag}\{a_i\} \quad (22)$$

where

$$\begin{aligned} [K]_{ij} &= \tfrac{N}{\pi}\mathbf{a}^T I^{ij}\mathbf{a}, \qquad i,j = 1,\ldots,P \\ \left[I^{ij}\right]_{pq} &= \int_0^{2\pi} \tfrac{\omega^2 \mathcal{S}_s(\omega)^2}{\mathcal{S}_r(\omega)^2} \sin(\omega(\tau_p - \tau_i)) sin(\omega(\tau_q - \tau_j)) d\omega. \end{aligned} \quad (23)$$

The CRB for the range and depth are shown in figures 4 to 7, for signal and noise with flat spectrum in a bandwidth B,

$$\mathcal{S}_s(\omega) = S_0, \quad \mathcal{S}_n(\omega) = N_0, \qquad |\omega| < 2\pi B. \quad (24)$$

The following nominal values, that may correspond to a deep ocean situation, were used: velocity profile $v_0 = 1480$m/s, $g_0 = -.035\ s^{-1}$, $g_1 = .016\ s^{-1}$; duct depth $Y_{\mathrm{duct}} = 914$ m; bottom depth $Y_{\mathrm{bottom}} = 5000$ m. Tables V and VI give the geometries for which the CRB's were computed and the resulting values for the delays (s), attenuations, and delays' derivatives (s/m).

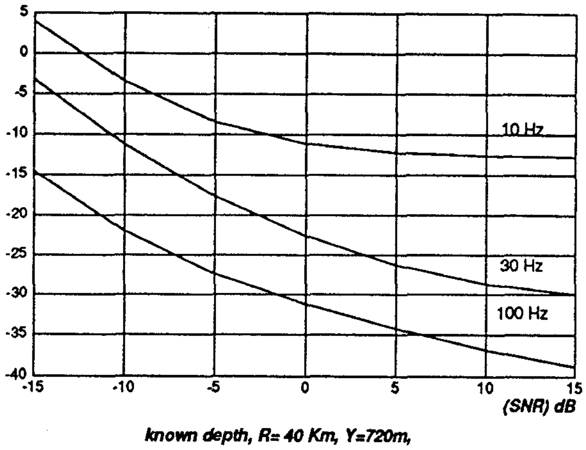

Figure 6: var(R)– Table VI. Known depth.

Table V — R = 55 Km; Y= 650m

	τ	a	$\partial\tau/\partial R$	$\partial\tau/\partial Y$
τ_1	36.7314	1.	$6.4947\ 10^{-4}$	$-3.4102\ 10^{-4}$
τ_2	36.905	-1.6	$6.5661\ 10^{-4}$	0.
τ_3	36.909	1.	$6.6204\ 10^{-4}$	0.
τ_4	36.9095	-1.6	$6.6127\ 10^{-4}$	0.
τ_5	36.9655	1.	$6.6658\ 10^{-4}$	$1.6188\ 10^{-4}$

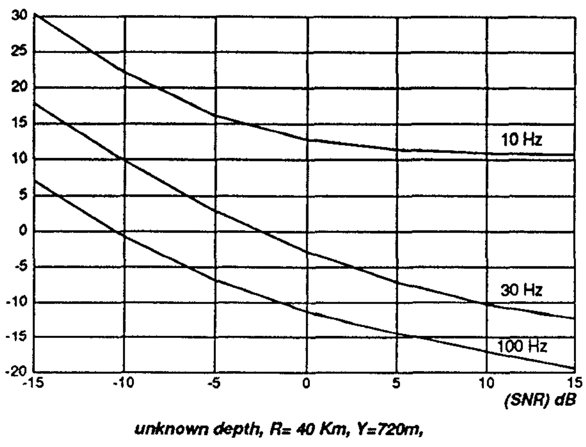

Figure 7: var(R)– Table VI. Unkown depth.

Table VI — R = 40 Km; Y= 720m

	τ	a	$\partial\tau/\partial R$	$\partial\tau/\partial Y$
τ_1	26.8718	1.	$6.56186\ 10^{-4}$	$-2.2392\ 10^{-4}$
τ_2	26.9288	2.	$6.6836\ 10^{-4}$	0.
τ_3	26.9449	1.	$6.7055\ 10^{-4}$	$1.0455\ 10^{-4}$

The plots show the normalized variances

$$\begin{aligned} \mathrm{var}(R) &= 10\ \log(\tfrac{N\ \mathrm{CRB}(R)}{R^2}) \\ \mathrm{var}(Y) &= 10\ \log(\tfrac{N\ \mathrm{CRB}(Y)}{Y^2}) \end{aligned} \tag{25}$$

as functions of the signal to noise ratio $\mathrm{SNR} \triangleq S_0/N_0$. We emphasize that due to the normalization by the (square of the) value of the parameters the plots display (the square of) relative errors. For a given value of the time – bandwidth product, i.e., of the number of data points, N, the values of the Cramer-Rao bounds $\mathrm{CRB}(\Theta)$ are given by the numerical values shown in the graphics translated by minus $10\log(N)$dB. Useful estimates correspond to values of the normalized CRB below 0 dB – which for $N \sim 100$ would correspond to relative errors in the order of 10%.

Since similar values for the normalized CRB's are obtained for range and depth, we chose to represent only the range CRB plots.

Conclusions

We summarize our conclusions:

1. Figures 5 and 7 show that by resolving the multiple interpath delays it is possible to determine both range and depth with a single sensor.

2. This in turn requires that the source signal bandwidth be large enough to separate the pathes – see figure 7 where a bandwidth larger than 30 Hz is required to get the bounds below 0 dB.

3. It is interesting to observe that for large ranges the complex ray structure corresponding to the bilinear profile significantly departs from the one predicted by the isovelocity model with straight pathes. Thie bilinear model can lead to the presence of useful interpaths delays, even between purely refracted rays.

4. Using the isovelocity model of [3] with a direct and a surface reflected path with the geometry of Table V, for a 10 Hz signal, the range CRB stays always above 0 dB, while figure 4 shows for the bilinear model an asymptotic CRB of -20 dB.

5. For small bandwidths, when only one interpath delay is efficiently resolved, with one sensor we can still estimate range (depth) if depth (range) is known –see plots 4 and 6.

6. The isovelocity model with a reflected and a refracted pathes predicts a monotonic improvement of the CRB's with depth, while that is not at all clear with the bilinear profile.

This work is a step in the direction of analyzing the impact on localization performance of depth inhomogeneity. It remains as a topic of further study the implications of range dependency of the velocity profile on the performance of localization systems.

References

[1] A. B. Baggeroer, W. A.Kuperman, and H. Schmidt. Matched field processing : source localization in correlated noise as an optimum parameters estimation problem. *J. Acoust. Soc. Am.*,2,571–587, 1988.

[2] C. S. Clay. Optimum time domain signal transmission and source location in a waveguide. *J. Acoust. Soc. Am.*, 81:660–664, 1987.

[3] B. Friedlander. Accuracy of source location using multipath delays. *IEEE Trans. on Aerosp. and Electr. Syst.*, Vol. 24, No. 4:346–359, 1988.

[4] D. F. Gingras. The effect of mismatch on array processors with normal mode steering vectors. In *Underwater Acoustics Data Processing*, Ed. Y. T. Chan, Kluwer Academ. Publ., 1988.

[5] M. J. Hinich. Maximum likelihood estimation of the position of a radiating source in a waveguide. *J. Acoust. Soc. Am.*, 66:480–483, 1979.

[6] John P. Ianiello. Large and small error performance limits for multipath time delay estimation. *IEEE Trans. on Acoustic, Speech and Signal Processing*, Vol. ASSP-34, No.2:245–251, April 1986.

[7] J. M. F. Moura and M. J. D. Rendas. Optimal filtering in the presence of multipath. In C. R. Baker, editor, *Stochastic Processes in Underwater Acoustics, Lecture Notes in Control and Information Sciences # 85*, pages 64–94. Springer-Verlag, N.Y., 1986.

[8] José M. F. Moura and M. João Rendas. Sensitivity of range localization in a multipath environment. In *Proceedings of the 1989 ICASSP.* IEEE, 1989.

[9] José M. F. Moura and Arthur B. Baggeroer. Passive systems theory with narrow -band and linear constraints: Part I – spatial diversity. *IEEE J. of Oceanic Eng.*, Vol. OE-3, No.1:5–13, Jan. 1978.

[10] H.L. Van Trees. *Detection, Estimation, and Modulation Theory.* John Willey & Sons, Inc., 1968.

[11] P. Whittle. The analysis of multiple stationary time series. *J. Royal Statist. Soc.*, Vol.15, 1953.